

# INDC International Nuclear Data Committee

## Neutron Inelastic Scattering Cross Sections on $^{16}\text{O}$ and $^{28}\text{Si}$

M. Boromiza<sup>a</sup>, C. Borcea<sup>a</sup>, Ph. Dessagne<sup>b</sup>, G. Henning<sup>b</sup>, M. Kerveno<sup>b</sup>, A. Negret<sup>a</sup>,  
M. Nyman<sup>c</sup>, A. Olacel<sup>a</sup>, and A. J. M. Plompen<sup>c</sup>

<sup>a</sup> Horia Hulubei National Institute for Physics and Nuclear Engineering, Bucharest-Măgurele, Romania

<sup>b</sup> Université de Strasbourg, IPHC, 23 Rue du Loess, 67037, Strasbourg, France

<sup>c</sup> European Commission, Joint Research Centre, Geel, Belgium

February 2020

Selected INDC documents may be downloaded in electronic form from  
<http://www-nds.iaea.org/publications/>  
or sent as an e-mail attachment.

Requests for hardcopy or e-mail transmittal should be directed to  
[nds.contact-point@iaea.org](mailto:nds.contact-point@iaea.org)  
or to:

Nuclear Data Section  
International Atomic Energy Agency  
Vienna International Centre  
PO Box 100  
A-1400 Vienna  
Austria

Produced by the IAEA in Austria  
February 2020

## Inelastic Scattering Cross Sections on $^{16}\text{O}$ and $^{28}\text{Si}$

M. Boromiza<sup>a</sup>, C. Borcea<sup>a</sup>, Ph. Dessagne<sup>b</sup>, G. Henning<sup>b</sup>, M. Kerveno<sup>b</sup>, A. Negret<sup>a</sup>,  
M. Nyman<sup>c</sup>, A. Olacel<sup>a</sup>, and A. J. M. Plompen<sup>c</sup>

<sup>a</sup> Horia Hulubei National Institute for Physics and Nuclear Engineering, Bucharest-Măgurele, Romania

<sup>b</sup> Université de Strasbourg, IPHC, 23 Rue du Loess, 67037, Strasbourg, France

<sup>c</sup> European Commission, Joint Research Centre, Geel, Belgium



February 2020



# Neutron inelastic scattering cross sections on $^{16}\text{O}$ and $^{28}\text{Si}$

*M. Boromiza<sup>a</sup>, C. Borcea<sup>a</sup>, Ph. Dessagne<sup>b</sup>, G. Henning<sup>b</sup>, M. Kerveno<sup>b</sup>, A. Negret<sup>a</sup>, M. Nyman<sup>c</sup>,  
A. Olacel<sup>a</sup>, and A. J. M. Plompen<sup>c</sup>*

<sup>a</sup>Horia Hulubei National Institute for Physics and Nuclear Engineering, Reactorului 30,  
077125, Bucharest-Măgurele, Romania

<sup>b</sup>Université de Strasbourg, IPHC, 23 Rue du Loess, 67037, Strasbourg, France

<sup>c</sup>European Commission, Joint Research Centre, B-2440 Geel, Belgium

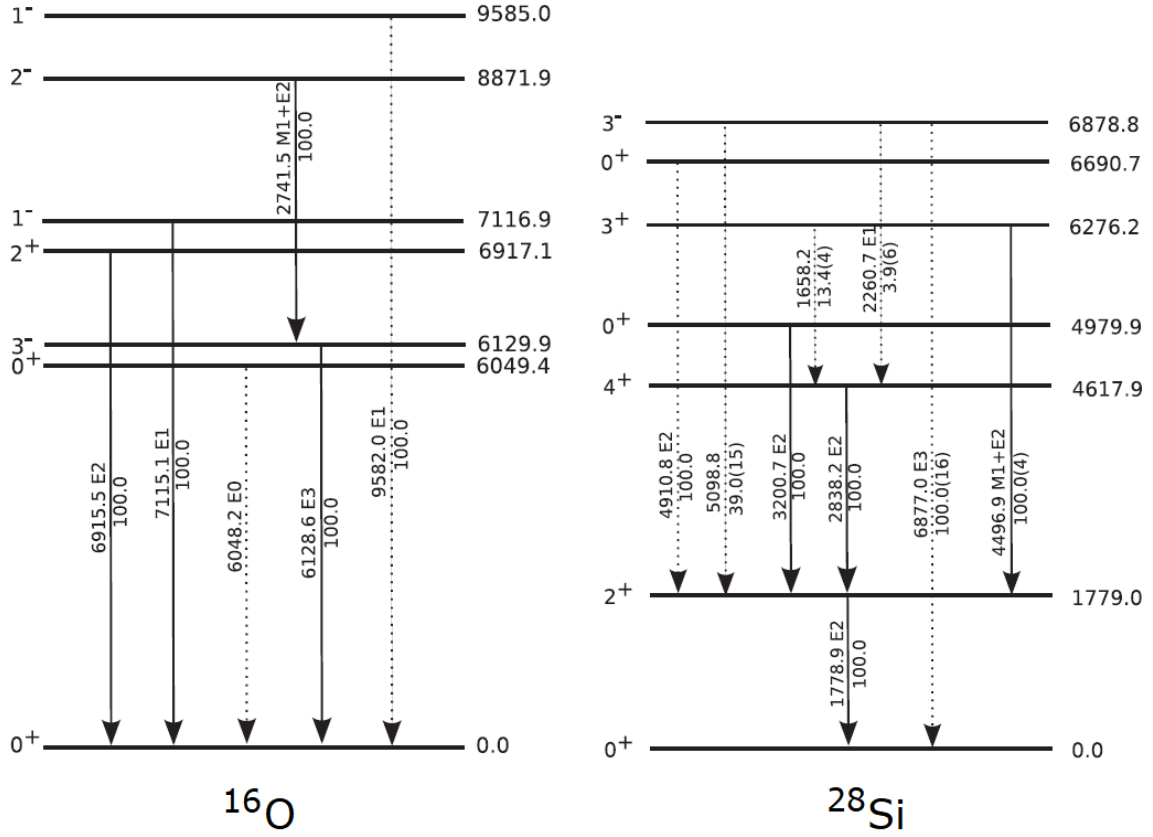
**Abstract.** Cross section measurements of the  $(n,n'\gamma)$  reaction on  $^{16}\text{O}$  and  $^{28}\text{Si}$  have been performed at the GELINA facility of JRC Geel. HPGe detectors were used for  $\gamma$ -ray detection. The scattering target was quartz ( $\text{SiO}_2$ ). Neutron-induced  $\gamma$ -production cross sections for all observed transitions in  $^{16}\text{O}$  and  $^{28}\text{Si}$  were determined, and the total inelastic cross section was calculated. This report provides the experimental details required to deliver the data to the EXFOR data library which is maintained by the Nuclear Data Section of the IAEA and the Nuclear Energy Agency of the OECD. The experimental conditions and data reduction procedures are described.

## 1. Introduction

In this report results of an inelastic neutron scattering cross-section measurement on  $^{16}\text{O}$  and  $^{28}\text{Si}$ , carried out at JRC Geel, are described. The results have been published in [1]. The experimental conditions and the data analysis procedures are described and further references given. A summary of the experimental details is given in Annex 1. In the description of the data the recommendations resulting from a consultant's meeting organized by the Nuclear Data Section of the IAEA have been followed [2].

The presence of oxygen in oxide reactor fuels and water and, by forming oxides, also as a structural material of nuclear reactors, makes accurate knowledge of neutron-induced reactions on  $^{16}\text{O}$  important. On the other hand, silicon is used as a component of the fuel rods and of the reflector in Gas-cooled fast reactors, which is one of the Generation IV reactor concepts. Partial level schemes for both  $^{16}\text{O}$  and  $^{28}\text{Si}$  are shown in **Figure 1** and the transitions for which  $\gamma$ -production cross sections were measured are indicated.

**Figure 1.** Partial level schemes of  $^{16}\text{O}$  and  $^{28}\text{Si}$ . The transitions for which  $\gamma$ -production cross sections were measured in the present experiment are drawn with solid arrows.



## 2. Experimental conditions and data reduction

### 2.1 The GELINA neutron source

The time-of-flight facility GELINA [3][4] has been designed and built for high-resolution cross section measurements in the resonance region. It is a multi-user facility, providing a pulsed white-neutron source with a neutron energy range from 10 meV to 20 MeV. Up to 10 experiments can be performed simultaneously at measurement stations located between 10 m to 400 m from the neutron production target. The electron linear accelerator provides a pulsed electron beam with an average energy of 100 MeV, a peak current of 12 A, and a repetition rate ranging from 50 Hz to 800 Hz. A compression magnet [5] reduces the width of the electron pulses to about 2 ns. The electron beam hits a mercury-cooled uranium target producing bremsstrahlung and subsequently neutrons via photonuclear reactions [6][7][8]. Two water-filled beryllium containers mounted above and below the neutron production target are used to moderate the neutrons. By applying different neutron beam collimation conditions, experiments can use either a fast or a moderated neutron spectrum – the fast spectrum being the one used in inelastic neutron scattering experiments. A view from the neutron production target position towards flight path 3, at 90° with respect to the GELINA electron beam direction, is shown in **Figure 2**. The collimation for the fast neutron spectrum on flight paths 1 and 3 is visible in front of the shutters, as are the shadow bars blocking the fast neutrons on flight paths 2, 4, 5, and 6. In the measurement reported here GELINA was operated at 800 Hz.

**Figure 2.** A view from the neutron production target position towards the north-side flight paths.

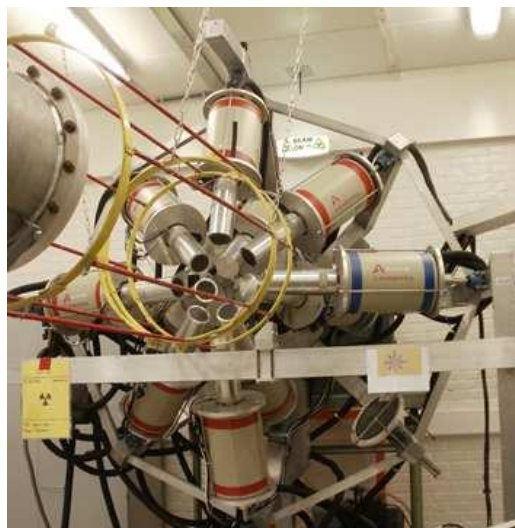


## 2.2 Experimental setup at flight path 3

The GAINS spectrometer, shown in

**Figure 3**, consists of 12 HPGe detectors mounted symmetrically around the sample position at backward angles ( $110^\circ$ ,  $125^\circ$ ,  $150^\circ$ ). There are four detectors at each angle. The HPGe detectors are coaxial, with similar crystal dimensions (80 mm diameter, 80 mm length). Ten detectors were equipped with a 0.5-mm carbon-epoxy entrance window, with the other two having a 0.5-mm aluminium window. The flight path length to the GAINS sample position is 198.757(5) m. The data acquisition system for the HPGe detectors uses Acquiris DC440 digitizers, which have a 12-bit amplitude resolution and a sampling rate of 420 million samples/s. A more detailed description of the data acquisition system is provided in [9].

**Figure 3.** The GAINS spectrometer.



The neutron flux was monitored with a  $^{235}\text{U}$  fission chamber, described in detail in [10]. The chamber was positioned 146.8 cm upstream of the sample position. The chamber contains eight  $\text{UF}_4$  deposits of 70 mm diameter, placed on five aluminium foils (20  $\mu\text{m}$  thickness). As the neutron beam diameter is smaller than that of the deposits, any inhomogeneity in the beam profile does not affect the neutron flux determination. The data acquisition for the fission chamber consists of analogue electronics. The time signal for each event was processed with a multi-hit fast time coder with a 0.5 ns time resolution [11]. The time and the pulse height of each detected event were recorded in list mode using a multi-parameter data acquisition system developed at JRC Geel [12]. The measurement station is equipped with air conditioning to reduce electronic drifts in the detection chains due to temperature changes.

The sample was a quartz ( $\text{SiO}_2$ ) cylinder. The physical properties of the sample, from measurements performed at JRC Geel, are summarized in **Table 1**. The sample mass was measured with a Mettler Toledo PG603-S balance, and the diameter and thickness with a vernier caliper.

**Table 1.** Physical properties of the  $\text{SiO}_2$  sample.

<b>Mass (g)</b>	322.81(72)
<b>Diameter (mm)</b>	76.26(4)
<b>Thickness (mm)</b>	32.30(4)

### 2.3 Data reduction

The experimental method is based on the detection of  $\gamma$  rays emitted following inelastic scattering of neutrons on the sample. The TOF technique is employed to determine the energy of the incident neutrons and the transitions are identified based on the measured  $\gamma$ -ray energies. A detailed account of the analysis procedure to extract the cross sections is given in [13], and an updated description of the fission chamber data analysis can be found in [10]. The neutron energy  $E_n$  is determined from the time-of-flight in the following manner:

$$E_n = E_0 \left[ \frac{1}{\sqrt{1 - \left(\frac{L}{ct}\right)^2}} - 1 \right] \quad (1)$$

where  $E_0$  is the rest mass of the neutron,  $L$  is the neutron flight path length,  $c$  is the speed of light in vacuum, and  $t$  is the neutron time-of-flight. A time reference is provided by the bremsstrahlung from the neutron-production target (the so-called  $\gamma$  flash), which is scattered from the sample into the detectors.

The list-mode data are sorted into  $E_\gamma$  vs. ToF matrices. The peak areas for the chosen  $\gamma$  rays are then determined for each ToF bin. This is done by summing the counts between the peak limits and subtracting a linear background based on the average background determined from each side of the peak. The determination of the  $\gamma$ -ray production cross section starts from the differential  $\gamma$ -production cross section  $d\sigma/d\Omega$ , which at neutron energy  $E_n$  for detector  $i$  positioned at an angle  $\theta_i$ , is given by

$$\frac{d\sigma}{d\Omega}(\theta_i, E_n) = \frac{1}{4\pi} \frac{Y_i(E_n)}{Y_{fc}(E_n)} \frac{\varepsilon_{fc}\sigma_U(E_n)}{\varepsilon_i} \frac{t_U}{t_s} \frac{A_s}{A_U} \frac{1}{c_{ms}(E_n)} \quad (2)$$

where  $Y_i(E_n)$  is the  $\gamma$ -ray yield,  $Y_{fc}(E_n)$  the fission chamber yield,  $\varepsilon_{fc}$  the fission chamber efficiency,  $\varepsilon_i$  the  $\gamma$ -ray detection efficiency,  $\sigma_U(E_n)$  the standard  $^{235}\text{U}(n,F)$  cross section, and  $t_U$ ,  $t_s$ ,  $A_U$ ,  $A_s$  the mass areal densities and atomic masses, respectively, of  $^{235}\text{U}$  in the fission chamber, and the sample under study. Finally,  $c_{ms}(E_n)$  is the correction factor for multiple neutron scattering, determined from Monte Carlo simulations. A Legendre polynomials series expansion of the differential cross sections from expression (2) coupled with the Gaussian quadrature method are then used to obtain the angle-integrated  $\gamma$ -production cross section. The total inelastic cross section is computed as a sum of the  $\gamma$ -production cross sections of transitions decaying directly to the ground state. Also, level cross sections are determined as the difference between the  $\gamma$ -ray production cross sections of the transitions depopulating the level and those feeding it. The method can only be applied reliably up to the highest level with at least one de-exciting  $\gamma$  ray observed in the experiment, and for which decay information is complete. Level cross sections with feeding missed in the experiment or in the decay scheme will be overestimated. In contrast, the total inelastic cross section will be underestimated in case no transitions are observed for levels that have a decay branch to the ground state.

The determination of the absolute  $\gamma$ -ray detection efficiency of the GAINS spectrometer relies on Monte Carlo simulations described in [14]. First, the  $\gamma$ -ray detection efficiency is determined experimentally with a  $^{152}\text{Eu}$  point source. An MCNP simulation is then performed and the model of the setup is adjusted until a satisfactory agreement between the experimental and simulated efficiencies is achieved. The final efficiencies are then determined by using the optimal detector geometry in a simulation in which the point source is replaced with a volume source corresponding to the size and material of the sample under study.

## 2.4 Uncertainties

The major components (correlated and uncorrelated) of the total experimental uncertainty of the  $\gamma$ -production cross sections are given in **Table 2** along with their typical values. There are additional correlated uncertainties arising from the other terms in Equation (2), but these are usually smaller. Considering all sources of uncertainty, the cross sections for the strongest channels have a typical total uncertainty of the order of 5%.

**Table 2.** Main components of the total uncertainty and their typical values in the experiment reported here.

Uncorrelated uncertainty (%)		Correlated uncertainty (%)	
HPGe efficiency calibration (statistics and MCNP simulation)	2	HPGe efficiency calibration ( $^{152}\text{Eu}$ source activity)	1.7
$\gamma$ -ray yield (strongest transitions)	5	Fission chamber efficiency	2
		$^{235}\text{U}(n,F)$ standard cross section	0.7
		Fission chamber yield	3

## Acknowledgements

This work was supported by the European Commission within the Seventh Framework Programme through Fission-2013-CHANDA (Project No. 605203) and EUFRAT (Project No. 211499). This work was also supported by the Ministry of Research and Innovation of Romania, CNCS-UEFISCDI, through the Project No. PN-III-P4-ID-PCE-2016-0025 within PNCDI III.

## References

- [1] M. Boromiza *et al.*, "Nucleon inelastic scattering cross sections on  $^{16}\text{O}$  and  $^{28}\text{Si}$ ", [\*Phys. Rev. C.\* \*\*101\*\* \(2020\) 024604](#).
- [2] F. Gunsing, P. Schillebeeckx and V. Semkova, Summary Report of the [Consultants' Meeting on EXFOR Data in Resonance Region and Spectrometer Response Function](#), IAEA Headquarters, Vienna, Austria, 8-10 October 2013, INDC(NDS)-0647 (2013).
- [3] A. Bensussan and J. M. Salomé, "GELINA: A modern accelerator for high resolution neutron time of flight experiments", [\*Nucl. Instr. Meth.\* \*\*155\*\* \(1978\) 11 – 23](#).
- [4] W. Mondelaers and P. Schillebeeckx, "GELINA, a neutron time-of-flight facility for neutron data measurements", [\*Notiziario Neutroni e Luce di Sincrotrone\* \*\*11\*\* \(2006\) 19 – 25](#).
- [5] D. Tronc, J. M. Salomé and K. H. Böckhoff, "A new pulse compression system for intense relativistic electron beams", [\*Nucl. Instr. Meth. A\* \*\*228\*\* \(1985\) 217 – 227](#).
- [6] J. M. Salome and R. Cools, "Neutron producing targets at GELINA", [\*Nucl. Instr. Meth.\* \*\*179\*\* \(1981\) 13 – 19](#).
- [7] M. Flaska *et al.*, "Modeling of the GELINA neutron target using coupled electron–photon–neutron transport with the MCNP4C3 code", [\*Nucl. Instr. Meth. A\* \*\*531\*\* \(2004\) 392 – 406](#).
- [8] D. Ene *et al.*, "Global characterisation of the GELINA facility for high-resolution neutron time-of-flight measurements by Monte Carlo simulations", [\*Nucl. Instr. Meth. A\* \*\*618\*\* \(2010\) 54 – 68](#).
- [9] L. C. Mihailescu, C. Borcea, and A. J. M. Plompen, "Data acquisition with a fast digitizer for large volume HPGe detectors", [\*Nucl. Instr. Meth. A\* \*\*578\*\* \(2007\) 298 – 305](#).
- [10] C. Rouki *et al.*, "High resolution measurement of neutron inelastic scattering cross-sections for  $^{23}\text{Na}$ ", [\*Nucl. Instr. Meth. A\* \*\*672\*\* \(2012\) 82 – 93](#).
- [11] S. de Jonge, "Fast Time Digitizer Type 8514 A", Internal Report GE/DE/R/24/87, CBNM Geel (1987).
- [12] J. Gonzalez, C. Bastian, S. de Jonge, and K. Hofmans, "Modular Multi-Parameter Multiplexer MMPM. Hardware description and user guide", Internal Report GE/R/INF/06/97, IRMM Geel (1997).
- [13] L. C. Mihailescu, L. Oláh, C. Borcea, and A. J. M. Plompen, "A new HPGe setup at Gelina for measurement of gamma-ray production cross-sections from inelastic neutron scattering", [\*Nucl. Instr. Meth A\* \*\*531\*\* \(2004\) 375 – 391](#).
- [14] D. Deleanu *et al.*, "The gamma efficiency of the GAINS spectrometer", [\*Nucl. Instr. Meth A\* \*\*624\*\* \(2010\) 130 – 136](#).

## Annexes

### Annex 1. Summary of experimental details

<b>1. Main reference</b>		[1]
<b>2. Facility</b>	GELINA, flight path 3 (200 m)	[3][4][5]
<b>3. Neutron production</b> Neutron production beam Nominal average beam energy Nominal average current Repetition rate (pulses per second) Pulse width Primary neutron production target Target nominal neutron production intensity	Electron 100 MeV 100 $\mu$ A 800 2 ns Depleted uranium with 10wt% Mo $3.4 \times 10^{13}$ neutrons/s	[6][7][8]
<b>4. Moderator</b> Primary neutron source position in moderator Moderator material Moderator dimensions (internal) (thickness, height $\times$ width $\times$ depth,...) Density (moderator material) Temperature (K) Moderator-room decoupler (Cd, B, ...)		
<b>5. Other experimental details</b> Measurement type Method (total energy, total absorption, ...) Flight path length from source to scattering sample (m) Flight path direction Neutron beam dimensions at sample position Neutron beam profile Overlap suppression Other fixed beam filters	(n,n' $\gamma$ ) $\gamma$ -ray detection, ToF 198.757(5) 90° to the electron beam 6.1(1) cm diameter  None ~2 cm depleted uranium to reduce the $\gamma$ flash	
<b>6. Detectors</b> Type Material Surface Dimensions Thickness (mm) Distance from sample (m) Detector(s) position relative to neutron beam Detector(s) solid angle	Number of detectors: 12 Semiconductor HPGe Coaxial, ~80 mm diameter 80 ~0.18 Backward angles: 110°, 125°, 150°	
<b>7. Sample</b> Type (metal, powder, liquid, crystal) Chemical composition	Quartz Crystal SiO <sub>2</sub> (natural isotopic composition)	

Sample composition	53% $^{16}\text{O}$ , 47% $^{28}\text{Si}$	
Temperature	Room temperature	
Sample mass (g)	322.81(72)	
Geometrical shape (cylinder, sphere, ...)	Cylinder	
Surface dimension (diameter in mm)	76.26(4)	
Nominal thickness (mm)	32.30(4)	
Containment description	No containment	
Additional comment		
<b>8. Data reduction procedure</b>		[10][13]
Dead time correction	Negligible	
Background subtraction	Linear in peak integration	
Flux determination (reference reaction)	$^{235}\text{U}(\text{n},\text{F})$	[10]
Normalization		
Detector efficiency	Calibration measurements + MCNP	
Self-shielding	From MCNP simulations	
Time-of-flight binning	2.38 ns	
<b>9. Response function</b>		
Initial pulse	Gaussian	
Target / moderator assembly		
Detector	Gaussian	

## Annex 2. Data format

Column	Content	Unit	Comment
1	ToF	ns	Time of flight corresponding to $E_i$
2	$E_i$	keV	Low boundary of the energy bin
3	$\sigma_{\text{exp}}$	b	Cross section (neutron energy bin $E_i \rightarrow E_{i+1}$ )
4	Total Uncertainty	b	
5	Increased total uncertainty	b	Additional uncertainty component, applicable to the 6915 keV transition only. See Ref. [1] for details.



---

Nuclear Data Section  
International Atomic Energy Agency  
P.O. Box 100  
A-1400 Vienna  
Austria

---

e-mail: [nds.contact-point@iaea.org](mailto:nds.contact-point@iaea.org)  
fax: (43-1) 26007  
telephone: (43-1) 2600 21725  
Web: <http://www-nds.iaea.org/>